Communications in Physics, Vol. 33, No. 2 (2023), pp. 123-132
DOI: https://doi.org/10.15625/0868-3166/17928

Generation and application of four-wave mixing in collinear high harmonic generation

Dinh Ba Khuong[1,2,†], **Tran Anh Khoa**[1], **Chau Huy Thong**[2], **Truong Vi Khanh**[1], **Nguyen Ba Hoi**[3], **Nguyen Tan Hung**[1], **Ho Phuoc Tien**[4] **and Dao Van Lap**[2]

[1]*Advanced Institute of Science and Technology, The University of Danang, Danang, Vietnam*
[2]*Optical Sciences Centre, Swinburne University of Technology, Vic 3122, Australia*
[3]*The University of Danang, Danang, Vietnam*
[4]*The University of Danang - University of Science and Technology, Danang, Vietnam*

E-mail: [†]kdinh@swin.edu.au

Received 4 December 2022; *Accepted for publication 1 February 2023*
Published 21 April 2023

Abstract. *We describe a thorough study of the wave-mixing procedure in the extreme ultraviolet (XUV) region involving three laser fields (800 nm, 1400 nm and 1860 nm). In addition to the phase matched high harmonic generation (HHG) spectrum generated by an 800-nm laser (driving field), non-integer order wave-mixing spectra are produced when the driving field and the control field (1400 nm or 1860 nm) are collinearly focused into krypton gas. In addition, the simultaneous presence of three laser fields generates resolvable four-wave mixing (FWM) frequencies that clearly indicate the contribution of each control field. We also discuss an application of the FWM scheme to extend the HHG cutoff region and generate the XUV quasi-continuum spectrum.*

Keywords: four wave-mixing processes; high harmonic generation; free electron laser.

Classification numbers: 42.65.Hw; 42.65.Ky; 41.60.Cr.

1. Introduction

Ultrafast nonlinear four-wave mixing (FWM) and two-dimensional Fourier-transform spectroscopies are important tools for studying electronic, vibrational and relaxation dynamics in the optical regions and have the potential to provide direct information on internal electronic and molecular couplings [1]. When optical pulses are used, the electron dynamics and vibrational motion in molecules become accessible on a femtosecond time scale where the temporal resolution for tracking the dynamical evolution is limited by the frequencies of the laser fields [2]. By employing XUV and X-ray pulses in four wave-mixing processes, this technique allows us to effectively study the fundamental dynamics associated with valence and core-level electronic transitions [3–5].

High harmonic generation (HHG) and free electron laser (FEL), which can produce XUV pulses, can be acted as light sources for such FWM spectroscopies [6–11]. Indeed, transient grating configurations with intense 80 fs XUV pulses from FELs were developed to produce wave-mixing signals that can be used to study the dynamics of coherent excitations as molecular vibrations [6,7]. A similar scheme with a subfemtosecond XUV pulse train and two few-cycle near-infrared pulses in atomic helium has successfully demonstrated the possibility to observe and measure dynamics on electronic timescales in both the temporal and spectral domains [12]. Although tabletop HHG sources can produce very short XUV pulses, their relatively low intensity leads to pulse energies insufficient to support nonlinear processes independently. By combining HHG radiation with moderately intense femtosecond laser pulses, nonlinear four-wave mixing signals involving the XUV fields and femtosecond laser fields can be produced [8–11]. Because the spectrum of the output light in the presence of the IR pulse is different from that of the phase-matched HHG radiation, a background-free FWM measurement can be realized [13].

Our group has used two multi-cycle laser fields with incommensurate frequencies to study FWM in the XUV region based on high harmonic generation from argon gas [9–11]. We also showed that the two-dimensional spectrum can be used to extract the amplitude and phase modifications of the atomic dipole moments of the coupled states in atomic krypton interacting with the intense pulsed laser light [14].

In this study, we present a detailed study of the wave-mixing process in the extreme ultraviolet (XUV) region involving three laser fields (800 nm, 1400 nm and 1860 nm). Besides the phase matched HHG spectrum generated by an 800-nm laser (driving field), non-integer order wave-mixing spectra are produced when the driving field and the control field (either at 1400 nm or 1860 nm) are collinearly focused into a gas medium. In addition, the simultaneous presence of three laser fields generates resolvable four-wave mixing (FWM) frequencies to show clearly the contribution of each control field. We also demonstrate for the first time that phase-matched cascaded wave-mixing process with our two-color HHG scheme can extend the cutoff region and produce a denser spectrum in the XUV region. Our proposed method not only enables the generation of attosecond pulses with high photon flux energy, but also provides an ultrafast tool for the investigation of quantum effects in atomic and molecular systems.

2. Theoretical background

High harmonic generation is induced in an extreme condition in which an intense driving laser interacts with a medium. Strong electric field of the driving laser ionizes the medium which is consequently a superposition of atomic gas and free-electron plasma. Due to the dispersion of the interaction, a small phase-mismatch is required to efficiently produce harmonic frequency ($\Delta k_q \approx 0$, q is the harmonic order). This criterion is satisfied as long as the phase mismatch of the neutral atomic cloud counterbalances with that of the plasma. When such an optimal condition is obtained, the harmonic intensity of the qth harmonic order can be written as [15,16]

$$I_q \propto p^2 L^2 e^{\left(\frac{-\alpha_q L}{2}\right)} \times \frac{\frac{\sin^2 \Delta k q_L}{2} + \sinh 2\frac{\alpha q_L}{4}}{\left(\frac{\Delta k_q L}{2}\right)^2 + \left(\frac{\alpha q_L}{4}\right)^2}. \quad (1)$$

In Eq. (1), the re-absorption of the harmonic signal α_q by the gas medium is taken into account, p is the pressure of the gas medium, L is the interaction length. The use of a control field in combination with a strong driving field, which produces the HHG, induces four-wave mixing processes the XUV region. The intensity of these coherent nonlinear optical wave-mixing fields is [9, 10]

$$I_{mix} \propto I_q I_1^n I_2^n \chi^{(2n+1)} p^2 L^2 \sin c^2 \left(\frac{\Delta k_{mix}}{L_2} \right), \tag{2}$$

where I_1 and I_2 are the intensities of the driving field and the control field (the signal or the idler field). The phase mismatch for the generation of these mixing frequencies is $\Delta k_{mix} \simeq k_{mix} - kq \pm n(k_1 - k_2)$, where k_1, k_2, k_q and k_{mix} are the wave-vectors of the driving field, the control field, the qth-order harmonic and the mixing field, respectively.

3. Experiment

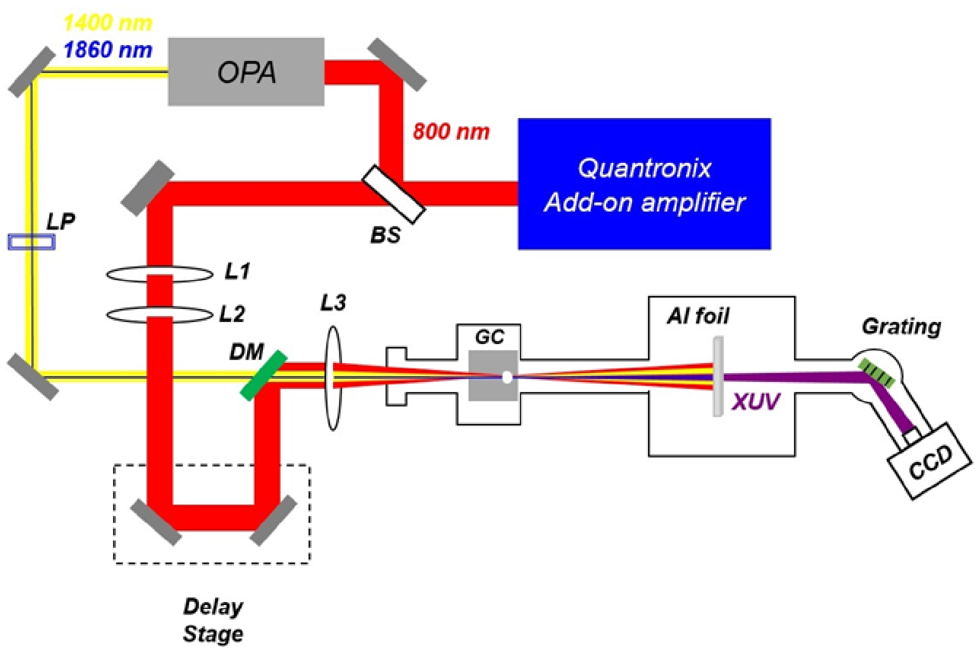

Fig. 1. Experimental setup. BS: beam splitter; OPA: optical parametric amplifier; LP: linear polarizer; L1, L2, L3: lenses; DM: dichroic mirror; GC: gas cell; XUV: emitted radiation; CCD: charge-coupled device.

Experiments for this study are performed at the Optical Sciences Centre, Swinburne University of Technology, Australia. A 1-kHz chirped-pulse amplifier system is used to provide 6.0 mJ, 800 nm, 30 fs laser pulses. A beam splitter is installed to divide the beam into two optical paths. The transmitted beam produces the high harmonic signals in a long cell filled with 25 torr of krypton gas. The reflected beam pumps an optical parametric amplifier (OPA) to create 0.6 mJ energy of two NIR control fields (signal field at 1400 nm and the idler field at 1860 nm). The intensity ratio of the signal to the idler wave is about 10:1. The HHG is generated by $\sim 1.2 \times 10^{14}$ W/cm^2 800-nm pulses and the two control fields are weak so that they do not create HHG radiation by themselves. The signal and the idler waves are polarized perpendicularly to each other; therefore a linear polarizer is used to control their presence in the interaction medium. In this configuration, a dichroic mirror is utilized to combine the driving and control beams so that they co-propagate before being focused into the gas cell by a 25-cm focusing lens. The phase-matching condition of the HHG is maintained during the experiment. A pair of lenses is used to manipulate the spatial overlap of the driving and the control fields. The delay time between these two fields is controlled by a DC motor, which has a 0.1 fs temporal resolution. Positive delay time implies that the first strong pulse, which drives the HHG, precedes the second weak pulse. The diameter of the beam spot at the focal plane is about150 µm. The krypton gas, which is contained in the cell, is isolated from the vacuum outside of the cell. On the back side of the gas cell, a small pinhole of roughly 150 µm, from which the XUV radiation propagates toward the detector, is drilled by the strong 800-nm driving beam. A 300-nm-thick aluminium foil is installed on the XUV beam path to neglect the fundamental beams. Positive delay time implies that the driving pulses precede the 800-nm control pulses.

4. Results and discussions

4.1. High harmonic generation

A HHG spectrum consisting of the harmonics H15 to H27 with 25-torr krypton gas at -300 fs delay is shown in Fig. 2. The iris controlling the diameter of the incident driving field and the relative position of the focusing lens to the cell's exit plane are iteratively manipulated to balance the effects of the neutral and plasma dispersions. As a result, an intense and narrow-bandwidth harmonic spectrum is observed when the intensity of the 800-nm field is $\sim 1.2 \times 10^{14}$ W/cm^2 and the focal plane is ~ 3 mm inside the cell. The dispersion caused by the generated free-electron plasma is effectively counterbalanced by the neutral dispersion. At a strong negative time delay of -300 fs, the control field has an insignificant effect on the HHG process. The inset of Fig. 2 shows the coherent spatial profiles of the three most intense harmonics H19 (green solid line), H21 (red dashed line), and H23 (blue dotted line). This indicates a high spatial coherence of the harmonic emission under our optimized experimental conditions.

The influence of phase mismatch on the HHG process is studied by varying the krypton gas density, which is shown in Fig. 3a. Initially, the experimental conditions are optimised at 25 torr so that a sharp HHG spectrum is obtained. The gas pressure is then varied from 5 torr to 150 torr, while the laser intensity and the focus position are kept constant. The spectral bandwidth and the sharpness of all harmonics are seen to be maintained during the measurement. In addition, the strength of the observable harmonics increases at a high rate as the input pressure increases from 5 torr to 25 torr. Fig. 3a shows that their intensities surpass the maximum values and then quickly decrease when the input pressure is higher than the optimal value. The data of H21 (red circles) extracted from Fig. 3a and the corresponding fitting curve (black dashed line) are shown in Fig. 3c. The good fitting line based on equation 1 implies that the phase-mismatch for the generation of H21 is small when $p_{Kr} \leq 25$ torr. In other words, an approximate p_{Kr}^2-dependence of the H21 intensity is realised in this pressure range. This is strong evidence of the phase-matched HHG process. When $p_{Kr} > 25$ torr, the phase-mismatch is larger leading to a rapid decline of the

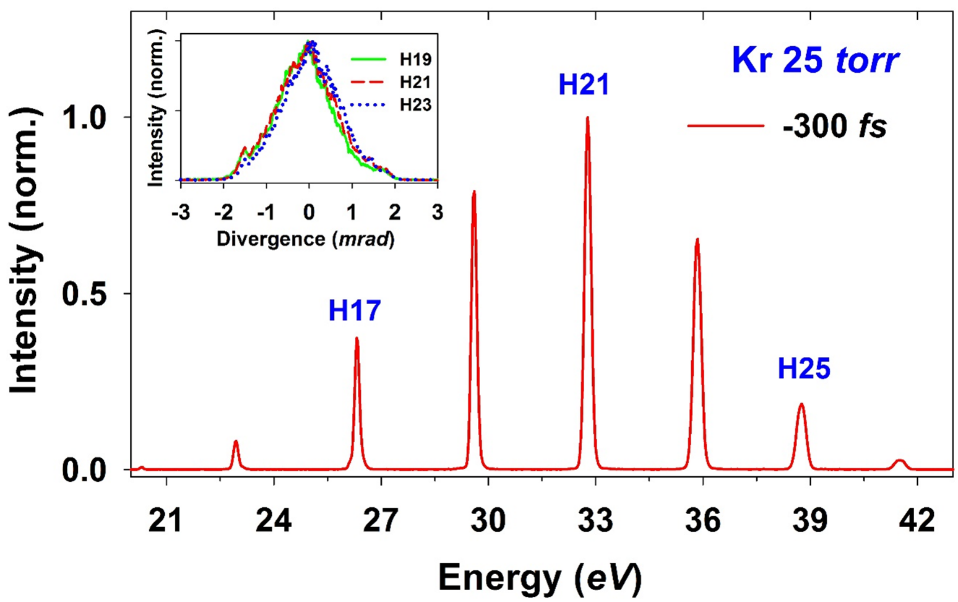

Fig. 2. (Color online) HHG spectrum with 25 torr krypton gas taken at time delay -300 fs. Inset: coherent far-field spatial profiles of the harmonics H19 (green solid line), H21 (red dashed line), and H23 (blue dotted line).

harmonic's intensity. The re-absorption effect of the neutral krypton gas becomes significant as $p_{Kr} > 40$ torr and therefore the harmonic H21 gradually decays with an exponential rate of pressure change. A similar dependence of other harmonics in the spectrum are also observed.

In another measurement, 25 torr of krypton is used as the interaction medium for the generation of a few intense harmonics. In Fig. 3b, the gas pressure and intensity of the driving field are unchanged, while the focal point is moved along the optical axis of the driving field to investigate the influence of the phase-mismatch on the harmonic strength. It is clear that when varying the focus position, the optical properties of all harmonics, e.g., spectral sharpness and bandwidth, are maintained. The negative, zero and positive values of the focus position indicate that the focal point is outside, at the exit plane, and inside of the gas cell, respectively.

Figure 3d shows the data for the strongest harmonic H21 (black triangles), which is extracted from figure 3b and its fitting curve based on Eq. (1). As the focus position x is -1.5 mm $< x \leq 3$ mm, the intensity of the H21 seems to go up with a quadratic effective interaction length L2. This is clear evidence that the HHG process has a small phase mismatch. Assuming that the effective interaction length is roughly equal to the focal shift over which the phase-matched HHG is produced, the H21 and other harmonics are coherently accumulated with a ~ 4 mm interaction length. As the lens moves deeper inside the cell ($x > +5$ mm), the HHG efficiency quickly decreases due to a large phase mismatch. As $x > +8$ mm, a familiar exponential decay of all harmonics is seen as a result of the predominant re-absorption in the krypton gas.

The intensity variation of all generated harmonics with respect to the gas pressure and the focus position discussed above indicates that the HHG fields with 25 torr krypton gas are produced under the phase-matched condition $(\Delta k_q \approx 0)$.

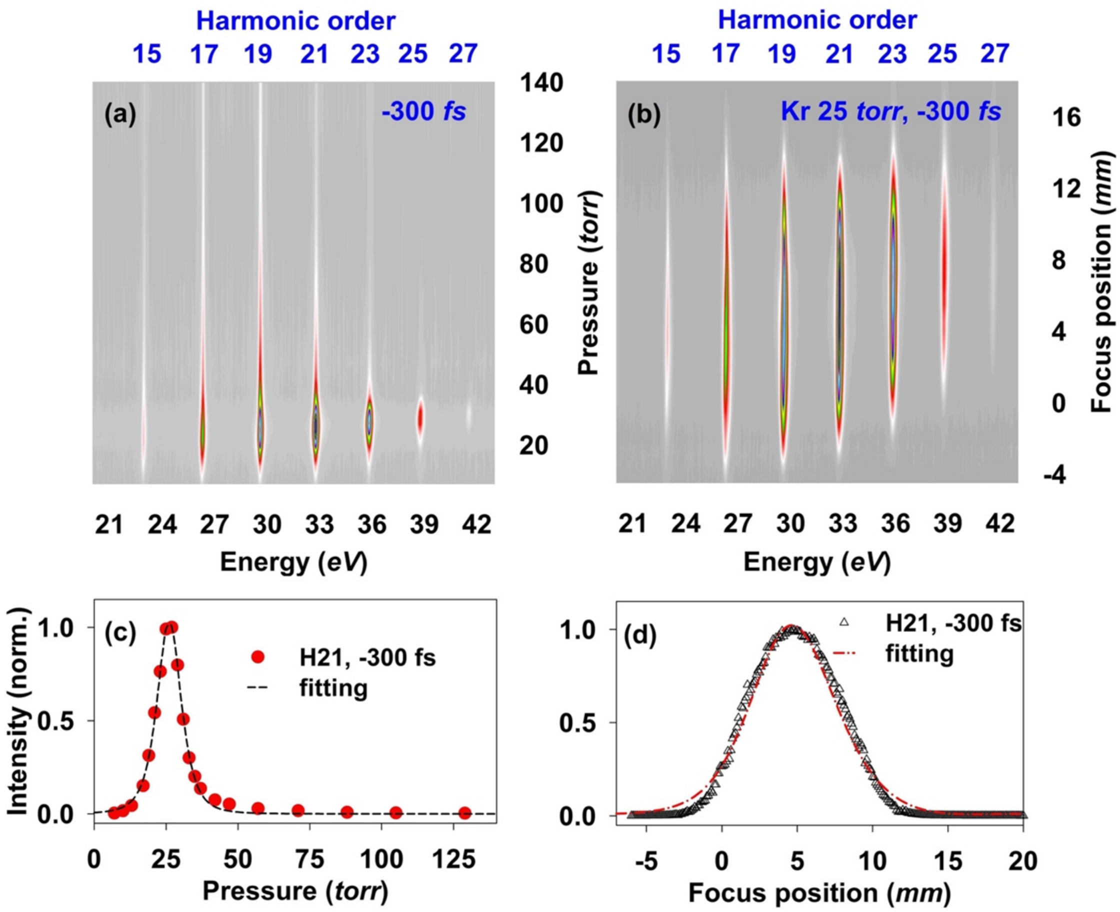

Fig. 3. (Color online) Illustration of the sharp HHG spectra taken at -300 fs time delay as a function of the krypton gas pressure (a) and the focus position (b). The experimental conditions are optimized with 25 torr krypton gas. The data of the harmonic H21 [red circles] (c) and [black triangles] (d) are taken from the two data sets (a) and (b), respectively. The black dashed line (c) and the red dash-dotted line (d) are the corresponding fitting curves of the harmonic H21.

4.2. Four-wave mixing in the XUV region

As discussed in subsection *4.1*, the control field (1400 nm or 1860 nm) does not affect the HHG process at a large time delay. As a result, the HHG spectrum only contains the odd harmonics at -300 fs (shown in Fig. 2). However, with two-color laser fields, perturbative nonlinear optical processes in the XUV region can be induced with a shorter delay. It is worth noting that the 1400 nm and the 1860 nm laser beam are polarized perpendicularly to each other. Thus, by using a linear polarizer and a half-wave plate, we can keep the relative polarization planes between the 800 nm and 1400 nm fields and between the 800 nm and 1860 nm fields parallel. Figure 4a shows the odd-order HHG spectrum (H15 to H27) and non-integer-order harmonics (sidebands of these odd harmonics) when either the signal field (1400 nm) or the idler field (1860 nm) overlaps in time (zero time delay) with the 800-nm field in the krypton gas. The polarization between the driving field and the control fields is parallel.

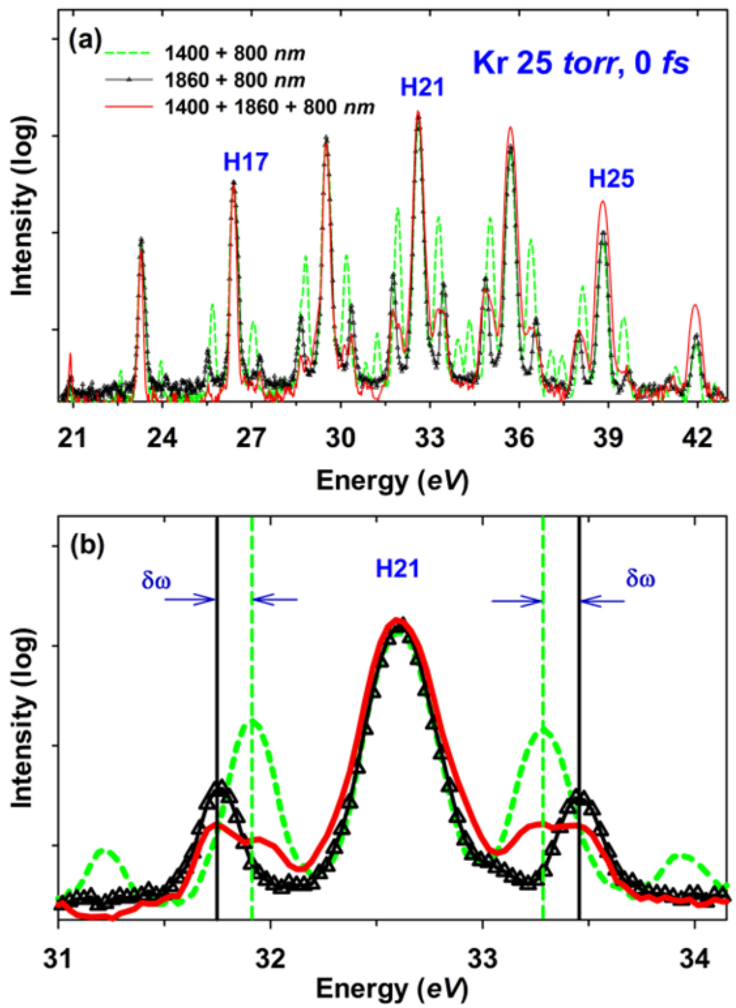

Fig. 4. (Color online) (a) Wave-mixing spectra of the 25 torr krypton gas at 0 fs time delay induced by two-color fields (800 nm and 1400 nm [green dashed line], 800 nm and 1860 nm [black triangles]), and three-color fields 800 nm, 1400 nm, and 1860 nm (red solid line). (b) The harmonic H21 and the mixing frequencies around this harmonic. Photon energy of the signal field $\omega_{1400} \cong 0.89$ eV, idler field $\omega_{1860} \cong 0.67$ eV; $\delta\omega \approx 0.24$ eV $\approx \omega_{1400} - \omega_{1860}$.

In this measurement, the experimental parameters for the generation of the sidebands (mixing frequencies) of the odd harmonics are adjusted so that the sharpness and bandwidth of the HHG spectrum at 0 fs are almost the same as those at -300 fs. Under these conditions, the intensity of the control fields is limited by $I_{1400} < 5 \times 10^{13}$ W/cm^2 and $I_{1860} < 5 \times 10^{12}$ W/cm^2. When the polarization of the driving and control beams is parallel, the most intense mixing peaks are observed at 0 fs time-delay between the 800-nm and 1400-nm fields (green dashed line) and between the 800-nm and 1860-nm fields (black triangles). It is worth reminding that the generation of the mixing fields is due to the perturbative nonlinear optical processes in the medium. Furthermore, the intensity of the mixing fields is directly proportional to the intensity of the control fields I2 (see Eq. (2)). Therefore, the mixture of the 800 nm (ω_{800}) and the 1400 nm (ω_{1400}) produce more mixing frequencies than the 800 nm and the 1860 nm (ω_{1860}). In addition, the mixing fields induced by the 800 nm and 1400 nm fields are stronger than those induced by the 800 nm and 1860 nm fields. Figure 4b shows the harmonic H21 and its mixing fields for a better visualisation of the energy calibration. On one side of each odd harmonic, the energy differences between the odd harmonic and the first mixing-order and between the first mixing-order and the second mixing-order induced by the 800-nm field and the 1400 nm field are about 0.67 eV and 2×0.67 eV, respectively (green dashed line, figure 4b). These two energy values are approximately $\Delta\omega$, and $2\Delta\omega$, where $\Delta\omega = \omega_{800} - \omega_{1400}$. Similarly, the energies of the mixing orders induced by the 800-nm field and the 1860 nm field can be measured at 0.89 eV (black triangles, figure 4b), which is approximately equal to $\Delta\omega' = \omega_{800} - \omega_{1860}$. Therefore, when the driving field (800 nm) and the control field (1400 nm or 1860 nm) overlap in time, the generated mixing frequencies can be expressed as $\omega_{mix} \cong \omega_q \pm n\Delta\omega$ (or $\omega_q \pm n\Delta\omega'$), where $n = 1$ or 2. This exhibits the energy conservation of the sum-frequency mixing and difference-frequency mixing processes in the XUV region. It is useful to recall that the phase variation of the fundamental field in the presence of free electrons is transferred to the harmonic field due to the nonlinear process of harmonic generation. Moreover, the influence of the plasma and neutral dispersions on the propagation of the XUV fields is small [17] leading to the fact that the harmonic phase is almost constant over the interaction length. The gas pressure is also low, so the dispersion of the driving field is similar to that of the control filed. Consequently, the phase mismatch of the mixing fields Δ kmix is close to zero. In other words, the phase-matching condition for the frequency-mixing processes is also satisfied.

We then investigate the optical wave mixing in the XUV region using a collinear scheme involving three fundamental laser fields. Here, the experimental conditions for the generation of HHG with the 800-nm field are the same as previously described. The two control fields (1400 nm and 1860 nm) are now focused simultaneously into the interaction medium when the polarizer's transmission axis is about 150 to the polarization plane of the 1860 nm field. With the presence of three fields of 800 nm, 1400 nm and 1860 nm, a broader mixing spectrum (red solid line in figure 4b) is generated. This spectrum clearly demonstrates two distinguishable FWM frequencies ($\omega_q \pm \Delta\omega$ and $\omega_q \pm \Delta\omega'$) on each side of each odd harmonic. The energy differences between the odd harmonic and the first mixing orders are measured at $\Delta\omega = \omega_{800} - \omega_{1400} \sim 0.67$ eV and $\Delta\omega' = \omega_{800} - \omega_{1860} \sim 0.89$ eV, respectively. In addition, the energy gap between the two vertical lines is $\delta\omega \approx \omega_{1400} - \omega_{1860} \cong 0.24$ eV.

It has been shown that we observe the same mixing fields in two cases of the two-color and three-color lasers. Their energies and momenta also obey energy and momentum conservation laws. In other words, our experimental data provide clear evidence for perturbative wave-mixing mechanism in the XUV region.

5. Generation of XUV quasi-continuum spectrum

Figure 4 shows that the spectral gap between two successive odd-harmonics driven by the 800-nm field is narrowed with an applied second field. According to the allowed photon combination $\omega_{mix} \cong \omega_q \pm n\Delta\omega$ that is discussed above, the shorter the wavelength of the control field, e.g.,

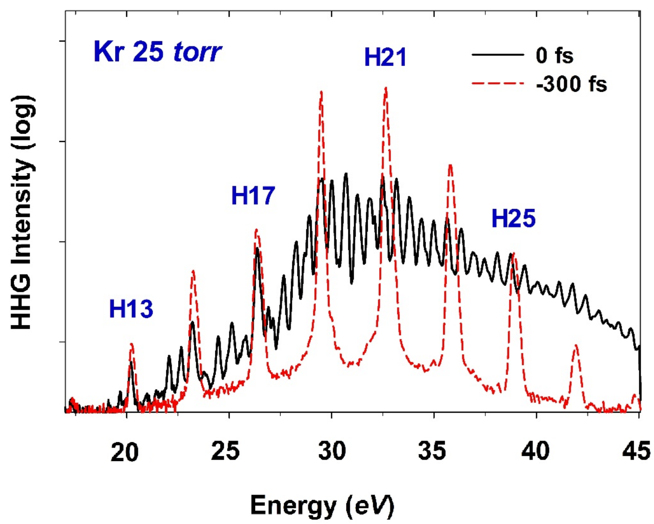

Fig. 5. (Color online) Generation of a quasi-continuum spectrum in the XUV region with the two-color HHG method. The spectral gap between two odd-harmonics (red dashed line, -300 fs) is filled with mixing-frequencies (blue solid line, 0 fs).

lesser 1400 nm, the smaller the gap between the mixing peaks. However, it is worth noting that the temporal profile of the generated pulses with a two-color HHG is demonstrated to reach a minimum with the IR field ranging from 1300 nm to 1400 nm [18]. Therefore, by increasing the intensity of the control field (the OPA signal field), a quasi-continuum spectrum is observed, as seen in Fig. 5. Such a denser spectrum could be attributed to the higher response of the nonlinear interaction medium. This method might thus be useful for the generation of attosecond pulses, which was recently studied by Takahashi *et al.* [18], when a proper intensity of the second field is used.

In Fig. 5, it is also clear that the harmonic generation in the cutoff region (> 45 eV) is enhanced leading the extension of the HHG cutoff energy with the use of two-color laser fields (800 nm and 1400 nm). The estimated cutoff energy of the two-color HHG is given by [18]

$$\hbar\omega_{cutoff}\omega_1 + \omega_2 \simeq I_p + 3.17Up1\left[1 + 1.6\sqrt{\xi}\frac{\omega_1}{\omega_2}\right] + 3.17U_{p1}, \tag{3}$$

where I_p is the binding energy of the electrons, $\xi = \frac{I_2}{I_1}$ is the intensity ratio between the control field ω_2 and the driving field ω_1, U_{p1} and U_{p2} are the ponderomotive potentials induced by the driving field and the control field, respectively.

6. Conclusion

We have discussed the generation of phase-matched four-wave mixing processes in the XUV region using a semi-finite gas cell and multiple color collinear femtosecond laser fields. A strong near-infrared laser at 800-nm was used to generate the phase-matched HHG radiation and a weak infrared control field (the signal or the idler field of an optical parametric amplifier) was then temporally and spatially synchronized with the driving field into in the krypton gas cell to induce new non-integer-order harmonics. Our experimental studies have revealed evidence of perturbative nonlinear optical wave-mixing processes in this spectral region. We have also for the first time reported a possible application of this four-wave mixing scheme in the extension of the HHG cutoff region and the generation of XUV quasi-continuum spectrum. This result paved the way to produce isolated attosecond XUV pulses for inner-shell absorption spectroscopy.

Acknowledgement

This work is supported by the Ministry of Education and Training, Vietnam (grant number B2022-DNA-06).

Conflict of interest

The authors have no conflict of interest to declare.

References

[1] S. Mukamel, *Principles of Nonlinear Optical Spectroscopy*, Oxford University, Oxford, 1999.

[2] A. M. Brańczyk, D. B. Turner and G. D. Scholes, *Crossing disciplines-A view on two-dimensional optical spectroscopy*, Ann. Phys. **526** (2013) 31.

[3] M. Lucchini, S. A. Sato, A. Ludwig, J. Herrmann, M. Volkov, L. Kasmi *et al.*, *Attosecond dynamical Franz-Keldysh effect in polycrystalline diamond*, Science **353** (2016) 916.

[4] M. Schultze, E. M. Bothschafter, A. Sommer, S. Holzner, W. Schweinberger, M. Fiess *et al.*, *Controlling dielectrics with the electric field of light*, Nature **493** (2013) 75.

[5] E. Goulielmakis, Z.-H. Loh, A. Wirth, R. Santra, N. Rohringer, V. S. Yakovlev *et al.*, *Real-time observation of valence electron motion*, Nature **466** (2010) 739.

[6] T. E. Glover, D. M. Fritz, M. Cammarata, T. K. Allison, Sinisa Coh, J. M. Feldkamp *et al.*, *X-ray and optical wave mixing*, Nature **488** (2012) 603.

[7] F. Bencivenga, R. Cucini, F. Capotondi, A. Battistoni, R. Mincigrucci, E. Giangrisostomi *et al.*, *Four-wave mixing experiments with extreme ultraviolet transient gratings*, Nature **520** (2015) 205.

[8] J. B. Bertrand, H. J. Wörner, H.-C. Bandulet, É. Bisson, M. Spanner, J.-C. Kieffer *et al.*, *Ultrahigh-order wave mixing in noncollinear high harmonic generation*, Phys. Rev. Lett. **106** (2011) 023001.

[9] L. V. Dao, K. A. Tran and P. Hannaford, *Cascaded four-wave mixing in the XUV region*, Opt. Lett. **43** (2018) 134.

[10] K. A. Tran, K. B. Dinh, P. Hannaford and L. V. Dao, *Phase-matched four-wave mixing in the extreme ultraviolet region*, *J. Appl. Phys.* **124** (2018) 015901.

[11] K. A. Tran, K. B. Dinh, P. Hannaford and L. V. Dao, *Phase-matched nonlinear wave-mixing processes in XUV region with multicolor lasers*, Appl. Opt. **58** (2019) 2540.

[12] A. P. Fidler, S. J. Camp, E. R. Warrick, E. Bloch, H. J. B. Marroux, D. M. Neumark *et al.*, *Nonlinear XUV signal generation probed by transient grating spectroscopy with attosecond pulses*, Nat. Commun. **10** (2019) 1384.

[13] W. Cao, E. R. Warrick, A. Fidler, S. R. Leone, and D. M. Neumark, *Near-resonant four-wave mixing of attosecond extreme-ultraviolet pulses with near-infrared pulses in neon: Detection of electronic coherences*, Phys. Rev. A **94** (2016) 021802(R).

[14] K. B. Dinh, K. A. Tran, P. Hannaford and L. V. Dao, *Four-wave mixing of extreme ultraviolet pulses and infrared pulses for studies of atomic dynamics*, J. Opt. Soc. Am. B **36** (2019) 3046.

[15] S. Meyer, B. N. Chichkov, B. Wellegehausen and A. Sanpera, *Phase-matched high-order harmonic generation and parametric amplification*, Phys. Rev. A **61** (2000) 063811.

[16] C. G. Durfee III, A. R. Rundquist, S. Backus, C. Herne, M. M. Murnane and H. C. Kapteyn, *Phase Matching of High-Order Harmonics in Hollow Waveguides*, Phys. Rev. Lett. **83** (1999) 2187.

[17] C. H. García, J. A. P. Hernández, J. Ramos, E. C. Jarque, L. Roso and L. Plaja, *High-order harmonic propagation in gases within the discrete dipole approximation*, Phys. Rev. A **82** (2010) 033432.

[18] E. J. Takahashi, P. Lan, O. D. Mücke, Y. Nabekawa and K. Midorikawa, *Infrared two-color multicycle laser field synthesis for generating an intense attosecond pulse*, Phys. Rev. Lett. **104** (2010) 233901.